**INTERNATIONAL JOURNAL OF OPTIMIZATION IN CIVIL ENGINEERING**
***Int. J. Optim. Civil Eng.2025; 15(3): 447-468***

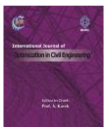

# OPTIMAL SEISMIC RETROFIT OF STEEL MOMENT-RESISTING MOMENT USING BRACING-FRICTION DAMPER SYSTEMS

M. Khatibinia[*, †], A.H. Saeedi, and E. Mohtashami
*Department of Civil Engineering, University of Birjand, Birjand, Iran*

## ABSTRACT

Bracing-friction damper system (BFDS), one of passive control devices, consists of a Pall friction damper added in-line with a diagonal, which is utilized for the seismic retrofit of building structures. The BFDS can dissipate the input energy of earthquakes and mitigate a considerable amount of the hysteretic energy of structures. This study presents the optimal seismic retrofit of inelastic steel moment-resisting frames (SMRFs) through the optimum design of the BFDSs installed in each story of SMRFs. For this purpose, minimizing the maximum damage index of stories averaged over seven scaled earthquake excitations is selected as the objective function so that the story damage is uniformly distributed along the height of SMRFs. The damage index is calculated based on the Park-Ang damage model which is expressed based on a linear combination of deformation, moment, and absorbed hysteretic energy of structural elements imposed by an earthquake excitation. The results indicate that the optimized BFDSs-equipped SMRFs exhibits the better distribution of story damage than that of uncontrolled SMRFs. Finally, the seismic assessment of SMRFs is done by the fragility analysis. The results of the seismic fragility assessment demonstrate that the optimized BFDSs improve the seismic performance of retrofitted SMRFs compared to that of uncontrolled SMRFs at different damage states.

**Keywords:** Optimum retrofit; bracing-friction damper system; Park-Ang damage model; damage distribution; seismic fragility assessment.

Received: 3 August 2025; Accepted: 29 September 2025

## 1. INTRODUCTION

Earthquakes, recognized as one of the most catastrophic natural events, impose a serious threat to human life and cause significant structural and economic losses. Given the wide-ranging socio-economic consequences and the destructive nature of seismic events,

[*]Corresponding author
[†]E-mail address: m.khatibinia@birjand.ac.ir (M. Khatibinia)

extensive research has been developed to both the seismic design of newly constructed buildings and the retrofitting of existing infrastructure [1-5]. To address and reduce the detrimental effects of seismic loading, various energy dissipation techniques have been introduced. Passive energy dissipation systems commonly referred to as passive control devices have gained notable attention due to their simplicity, reliability, and effectiveness. These systems primarily operate using the mitigation of the energy demand imposed on structural elements during an earthquake. In essence, passive devices are designed to either reflect or absorb a portion of the seismic input energy, thereby diminishing the level of hysteretic (plastic) energy dissipated by the structural components [6, 7]. As a result, these systems play a vital role in mitigating seismic vulnerability and preventing damage to both structural and non-structural elements of a building. Among the various categories of passive energy dissipation systems, friction dampers can dissipate seismic input energy into heat through frictional sliding between two surfaces [8-10]. While passive control systems are not inherently cost-effective in all cases, friction dampers stand out for their affordability and ease of implementation. Compared to other damping devices such as viscous or viscoelastic dampers, friction dampers not only offer sufficient lateral stiffness, but also exhibit hysteretic characteristics like to those of metallic yielding devices.

One of the most widely recognized models is the Pall friction damper which was first introduced by Pall and Marsh [8]. The Pall friction damper has been successfully implemented in both newly designed structures and retrofitted older buildings [11, 12]. Several connection configurations for these devices have been explored, including in-line arrangements with diagonal braces, as well as placements at the intersection points of X-bracing or chevron bracing systems. Moreover, advancements in friction damper technology have led to the development of several enhanced variants such as the improved Pall friction damper [13], Sumitomo friction damper [14], rotational friction damper [15], and friction walls [16]. FitzGerald et al. [17] proposed a novel application using slotted bolted connections (SBCs) within diagonal bracing systems. Monir and Zeynali [18] developed and experimental validated a modified friction damper positioned at the intersection of X-diagonal braces. Ebrahimi and Mirghaderi [19] designed a friction-slip damper located at the mid-span of square hollow structural sections (square-HSS) and H-shaped braces. Their findings indicated that the proposed damper effectively prevented strength and stiffness degradation in braces while enhancing their energy dissipation capacity. Additionally, several studies [20-24] have highlighted the advantages of installing friction dampers at beam-to-column joints in steel moment-resisting frames (SMRFs).

The optimal design of friction dampers has emerged as a complex yet essential topic within the field of structural engineering and has considerable been interested by researchers. Moreschi and Singh [25] investigated the optimal placement of friction dampers throughout various building levels and employed a genetic algorithm to determine key design parameters such as slip load and brace stiffness. Lee et al. [26] proposed a seismic design methodology for friction dampers based on the distribution of story shear forces in elastic structural systems. Taiyari et al. [27] developed a probability-based framework for designing chevron-braced friction dampers within SMRFs and utilized seismic fragility functions to evaluate structural vulnerability and damage likelihood. Furthermore, Ghorbani and Rofooei [28] introduced an innovative friction damping system with dual slip loads for enhancing the seismic performance of SMRFs. Their optimization process treated both the

slip force levels and the initial slip displacement as critical design variables. Jarrahi et al. [7] addressed the optimal design of rotational friction dampers for controlling inelastic behavior in single-story SMRF. Extending their previous work, Jarrahi et al. [29] explored the optimal distribution and design of rotational friction dampers for a 10-story inelastic frame subjected to earthquake ground motions. Additionally, Moghaddam et al. [30] developed an optimization strategy to simultaneously determine the ideal locations and slip forces of friction dampers, with the goal of enhancing the seismic performance of SMRFs across multiple performance levels.

In previous research efforts, various parameters such as structural responses and the amount of energy dissipated were frequently employed as objective indicators in the optimal design of friction dampers. However, these indices are inherently limited and often fail to consistently and comprehensively reflect the extent of structural damage resulting from seismic events. As such, there is a critical need to establish more robust and inclusive performance indicators and optimization constraints that more accurately represent actual structural damage. Another important shortcoming observed in the reviewed studies is that the optimization procedures have often been carried out subjected to a single earthquake record. Furthermore, none of the previous investigations has addressed the optimization of damage distribution along the height of a structure equipped with friction dampers. Feurther, the damage concentration in specific stories can lead to undesirable failure mechanisms during strong earthquake excitations.

This study addresses the gap identified above through the optimum design of bracing-friction damper systems (BFDSs) using the extent of seismic damage to the stories of a SMRF averaged over a number of scaled seismic excitations as the objective function. The uniform distribution of story damage over the height of the controlled SMRF is also considered as the constraint of the optimization problem. In addition, the parameters of the BFDSs are considered as the design variables. In order to determining the extent of seismic damage, the Park-Ang damage model is adopted and used in this study. Due to taking into account both maximum plastic displacement and plastic dissipated energy, this damage model can represent a good correlation with the observed damage status after occurring an earthquake. A modified particle swarm optimization (PSO) algorithm is used to solve the optimization problem. Finally, the fragility curves are developed to assess the seismic performance of the optimized BFDSs-equipped SMRF at different damage states.

## 2. BRACING-FRICTION DAMPER SYSTEMS (BFDS)

The BFDS depicted in Figure 1 integrates a Pall-type friction damper directly in-line with a diagonal brace. Its force-displacement behavior can be idealized as an elastic-perfectly plastic model characterized by a high initial stiffness. Under seismic loading, this system dissipates a portion of the input earthquake energy through frictional sliding between steel plates compressed by post-tensioned bolts, thereby reducing the energy transmitted to the structural elements [11]. As shown in Figure 1, the mechanical response of the BFDS can be divided into distinct operational phases. Initially, the system exhibits a stick–slip behavior before any relative movement occurs between the friction plates. This is followed by a steady sliding phase, during which energy is effectively dissipated through controlled

slippage. In cases of strong ground motion, an additional stage, referred to as the slip-lock phase, may emerge after the sliding phase. This condition arises when the bearing capacity of the post-tensioned bolts is activated and shows additional resistance to further displacement [31, 11].

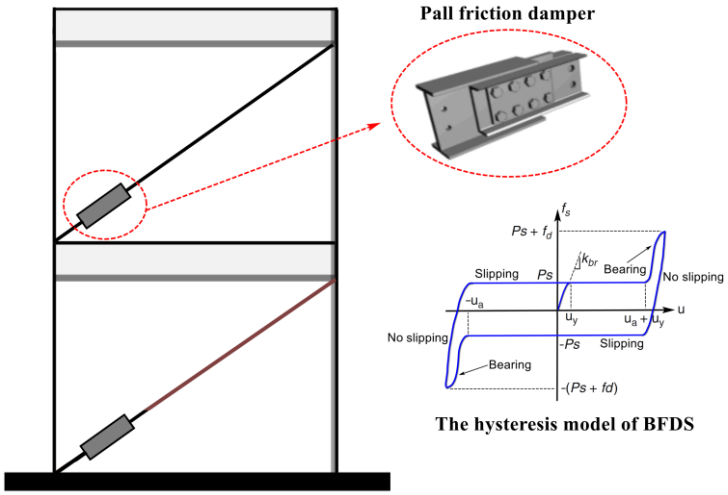


Figure 1: A frame equipped with BFDSs and the hysteresis model of a BFDS [11]

As shown in Figure 1, the friction damper is arranged in series with its corresponding diagonal brace, and the BFDS operates in parallel with the primary lateral-load-resisting components of the structure. Within the design philosophy of the BFDS, the brace element is expected to remain entirely within its elastic regime throughout seismic excitation, thereby ensuring that all energy dissipation occurs within the friction damper through controlled plate slippage. Referring to the idealized hysteretic behavior shown in Figure 1 during the initial stick-slip phase, the friction damper exhibits an elastic stiffness denoted by $k_d$, which is designed to be greater than the stiffness of the supporting brace element, $k_{br}$. This mechanical configuration leads to an effective or equivalent stiffness for the BFDS, represented by $k_{bd}$. The equivalent stiffness can be derived as a function of $k_d$ and $k_{br}$, and is given by the following relation [25, 27]:

$$k_{bd} = \frac{k_{br}k_d}{k_{br}+k_d} \xrightarrow{k_d \to \infty} k_{bd} = k_{br} \tag{1}$$

The slip force of the BFDS, $P_s$, is also obtained as:

$$P_s = k_{br}u_y = SRk_s u_y \quad ; \quad SR = \frac{k_{br}}{k_s} \tag{2}$$

where $k_s$ is the stiffness of story where the BFDS is installed in it. $u_y$ is the total slipping displacement (or the displacement of the brace at which the device starts to slip). Further, the slip force of the BFDS can be defined based on the weight of story as follows [27]:

$$P_s = \bar{F} W_s \tag{3}$$

where $\bar{F}$ is the normalized slip force pertinent to the BFDS device.

Two primary parameters govern the design of friction dampers in seismic applications: the stiffness ratio between the brace and the story (denoted as *SR*), and the normalized slip force. While several numerical strategies have been developed for determining the optimal slip force, their implementation remains computationally intensive, particularly for large-scale structural systems. Baktash and Marsh [32] proposed a numerical approach in which the optimal slip force is identified by minimizing the discrepancy between the input and dissipated energy throughout the structural response. In another study, Lee et al. [33] introduced two coefficients for distributing friction dampers along the building height. These coefficients were defined by normalizing the slip load with respect to the maximum shear demand and the peak inter-story shear force observed in the uncontrolled structure. Furthermore, in their methodology, the stiffness ratio, *SR*, was assumed to be fixed at a value of 2. It is important to highlight that although such numerical methods offer theoretical precision, their practical application to complex or multi-story buildings often incurs significant computational expense.

## 3. SEISMIC DAMAGE INDEX

The extent of structural deterioration resulting from seismic events can be effectively characterized through the use of a damage index (DI). The indices serve as quantifiable measures to evaluate both localized failures in individual structural elements and the overall integrity of the entire system across varying levels of seismic intensity. Numerous forms of DIs have been introduced, particularly tailored to assess the performance of reinforced concrete and steel frameworks [34-38]. Typically, a DI is formulated as a non-dimensional metric ranging from 0 to 1, where a value of 0 denotes a completely intact structure and a value of 1 signifies total structural failure or collapse. Intermediate values within this range correspond to varying degrees of partial structural degradation.

One of the most popular and practical DIs is the Park-Ang damage model ($DI_{\mathrm{PA}}$) [39] which has efficiently been adopted for the evaluation of the damage level in reinforced concrete and steel structures. Initially, $DI_{\mathrm{PA}}$ was formulated as a linear combination of peak displacement (often related to ductility) and the amount of energy dissipated through hysteresis. Nevertheless, because inelastic deformations predominantly occur within plastic hinge zones of certain structural members, establishing a direct link between global structural displacements, localized plastic rotations, and the DI remains a main challenge. Hence, $DI_{\mathrm{PA}}$ was modified later by Park et al. [38] and Kunnath et al. [37] to express damage in a structural element as a linear combination of its rotation, moment, and cumulative energy demand during earthquake excitation. For the element's end-section damage, the modified $DI_{\mathrm{PA}}$ is expressed as [40]:

$$DI_{\mathrm{PA}} = \frac{\theta_m - \theta_r}{\theta_u - \theta_r} + \frac{\beta}{\theta_u M_y} \int dE \tag{4}$$

where $\theta_m$ and $\theta_u$ are the maximum rotation of the end-section and ultimate rotation capacity of the structural element, respectively, $\theta_r$ is the recoverable rotation after unloading, $\beta$ is a non-negative parameter, $M_y$ is the yield moment of structural element, and $\int dE$ is the dissipation hysteretic energy of structural element.

The modified $DI_{\mathrm{PA}}$ is the basis of the story and overall damage indices [37]. These indices represent hysteretic energy dissipation in structural elements at the story and overall levels as:

$$DI_{\text{story}} = \sum_{i=1}^{Ne} (\lambda_{\text{component}})_i (DI_{\text{PA}})_i \quad ; \quad (\lambda_{\text{component}})_i = \left(\frac{E_i}{\sum_{i=1}^{Ne} E_i}\right)_{\text{component}} \tag{5}$$

$$DI_{\text{overall}} = \sum_{i=1}^{Ns} (\lambda_{\text{story}})_i (DI_{\text{story}})_i \quad ; \quad (\lambda_{\text{story}})_i = \left(\frac{E_i}{\sum_{i=1}^{Ns} E_i}\right)_{\text{story}} \tag{6}$$

where $DI_{\text{story}}$ and $DI_{\text{overall}}$ are the damage index of stories and overall structure, respectively. $E_i$ is the total absorbed energy (or absorbed hysteretic energy) by the $i$th structural element or story. $Ne$ and $Ns$ are the number of structural elements and stories, respectively. It is noted that in this study, the absorbed hysteretic energy of structural members is calculated using the approximate computing method introduced by Gong *et al*. [41].

## 4. OPTIMUM DESIGN OF BFDS DEVICES

In this study, the optimization problem focused on finding the parameters of the BFDSs in order to minimize the maximum $DI_{\text{story}}$ of an inelastic SMRF averaged over a predefined number of scaled earthquake excitations. The design parameters of the BFDSs included the stiffness ratio, $SR$, and the normalized slip force, $\bar{F}$. In this study, it was assumed that an BFDS was installed in each story of an $Ns$-story SMRF. Therefore, the optimization problem is defined as:

$$\begin{aligned}
&\text{Find}: \quad \mathbf{X} = \left\{SR_1, SR_2, \ldots, SR_{Ns}, \bar{F}_1, \bar{F}_2, \ldots, \bar{F}_{Ns}\right\} \\
&\text{Minimize}: \ f(\mathbf{X}) = \max\left[\frac{1}{Neq}\sum_{ie=1}^{Neq} DI_{\text{story},ie}\right]_{is} \quad ; \quad is = 1,2,...,Ns \\
&\text{subject to}: \ g_j(\mathbf{X}) \le g_{\text{all},j} \quad ; \quad j = 1,2,\ldots,n \\
&\qquad\qquad SR_i^{\min} \le SR_i \le SR_i^{\max} \quad ; \quad i = 1,2,\ldots,Ns \\
&\qquad\qquad \bar{F}_i^{\min} \le \bar{F}_i \le \bar{F}_i^{\max}
\end{aligned} \tag{7}$$

where $SR_i^{\min}, SR_i^{\max}, \bar{F}_i^{\min}$, and $\bar{F}_i^{\max}$ set bounds on the stiffness ratio and the normalized slip force of the $i$th BFDS; $g_j$ and $g_{\text{all},j}$ are behavioral constraints and their allowable values;

and *Neq* is the predefined number of scaled earthquake excitations, taken to be seven in this study.

The distribution pattern of the story damage index ($DI_{\text{story}}$) was considered as the constraint to prevent the concentration of damage during severe earthquake excitations and ensure a relatively uniform distribution of damage along the structure's height. The constraint was defined as follows [42]:

$$g_1 = \text{mean}(DI_{\text{story}})_i - \text{mean}(DI_{\text{story}})_j \le DI_{\text{all}} \quad ; \quad i = j = 1,2,...,Ns \tag{8}$$

where $DI_{all}$ is a user-defined value for the uniform distribution of $DI_{\text{story}}$.

The mean value of maximum force, $F_i^{\max}$, of the *i*th brace corresponding to *i*th BFDS averaged over seven scaled earthquake excitations was considered as another constraint:

$$g_2 = \frac{1}{Neq}\sum_{ie=1}^{Neq}(F_i^{\max})_{ie} \le F_{\text{all}} \quad ; \quad i = 1,2,\ldots,Ns \tag{9}$$

where $F_{\text{all}}$ is the ultimate axial capacity for tension or compression in accordance with AISC-LRFD.

A number of constraint-handling approaches have been proposed for solving optimization problems with metaheuristic optimization methods [43]. In this study, a dynamic penalty function was used as follows [44, 45]:

$$P_f = (1+\varepsilon_1 v)^{\varepsilon_2} \quad ; \quad v = \sum_j \max\left(\frac{g_j}{g_{j,\text{all}}} - 1, 0.0\right) \tag{10}$$

where $P_f$ is the penalization factor. $\varepsilon_1$ and $\varepsilon_2$ are parameters that determine the behavior of penalty function. In this approach, a penalty term is multiplied by the constrained objective function to convert it into an unconstrained one, $\tilde{f}$, as:

$$\tilde{f}(\mathbf{X}) = f(\mathbf{X}) \times P_f \tag{11}$$

In the present study, the particle swarm optimization (PSO) with passive congregation, proposed by He et al. [46], was used for the optimum design of the BFDSs installed in the stories of an inelastic SMRF.

## 5. SEISMIC FRAGILITY ASSESSMENT

Seismic fragility assessment of a building structure is defined as the conditional probability of exceeding a prescribed damage state (DM), given of intensity measure (IM). In other words, it describes the relationship between IM and DM and assesses the probability of failure of a structure under different earthquakes. The performance-based fragility analysis

method for a structure is to apply the performance-based seismic design method to a seismic fragility analysis [47, 48]. This method allows for assessing the probability of exceedance of each performance level at various levels of damage given a specific ground motion intensity.

Fragility curves represent the conditional probability of damage that structural seismic demand would reach or exceed a limit state. Within the performance-based design framework, this probability is conditioned on a given IM, here representing the level of ground shaking. The fragility function is expressed as [49]:

$$F = P\left[ C \geq D_{LS_i} \left| IM \right. \right] \tag{12}$$

where $C$ is the maximum response of the structure, and $D_{LS_i}$ is the capacity of a limit state corresponding to the structural response at the $i$th performance level.

The fragility function can be defined based on two assumption including: 1) a lognormal distribution for the response $C$; 2) a deterministic nature for the limit state capacity $D_{LS}$ per code requirements. Hence, the fragility function is expressed as [49]:

$$F = 1 - \Phi\left( \frac{\ln(D_{LS_i}) - \lambda_{C|IM}}{\beta_{Tot}} \right) \tag{13}$$

where $\Phi(\cdot)$ is the standard normal cumulative distribution function, $\lambda_{C|IM}$ is the natural logarithm of the median of the response in a specific intensity measure which is calculated by the estimated relationship between $IM$ and $C$; and $\beta_{Tot}$ is total uncertainty of the system encompassing uncertainties associated with capacity, modeling, and property of structures as [50]:

$$\beta_{Tot} = \sqrt{\beta_{RTR}^2 + \beta_{DR}^2 + \beta_{DT}^2 + \beta_{MDL}^2} \tag{14}$$

where $\beta_{RTR}$, $\beta_{DR}$, $\beta_{TD,}$ and $\beta_{MDL}$ are the uncertainty sources of record-to-record, design requirements, test data, and modeling, respectively. In the present study, the values of $\beta_{RTR}$, $\beta_{DR}$, $\beta_{TD}$, and $\beta_{MDL}$ were respectively assumed to be 0.4, 0.2, 0.2, and 0.1 [51].

Based on the results of the studies implemented by Cosenza and Manfredi [52] And Park et al. [53], $DI_{\text{overall}} \geq 1.0$ represents the collapse level, for $DI_{\text{overall}} \leq 0.5$ the damage is repairable, and for $0.5 < DI_{\text{overall}} < 1.0$ no collapse occurs in the building but the damage of the building is not repairable. Moreover, for $DI_{\text{overall}} < 0.2$ the damage is negligible. Pujades et al. [54] proposed the new thresholds for damage states which was used in this study. The limit states included the slight damage state at $DI_{\text{overall}} = 0.1$, the moderate damage state at $DI_{\text{overall}} = 0.2,$ and the severe damage state at $DI_{\text{overall}} = 0.4$ [54]. In addition, $DI_{\text{overall}} = 0.9$ was assumed as the complete damage state (i.e., not-repairable damage) in this study.

## 6. MODELLING INELASTIC SMRF EQUIPPED WITH BFDS

Two benchmark SMRFs shown in Figure 2 were used in this study to demonstrate the efficacy of the optimized BFDSs for the seismic retrofit of the structures. The three-bay, 6- and 10-story SMRFs were introduced by Wong [55] and Wong and Johnson [6], respectively. The mass of the 6- and 10-story SMRFs were assumed to be 300 and 218.9 tons, respectively. The beams of the SMRFs were subjected to a uniformly-distributed load of 21.89 kN/m. Structural damping was assumed to be 3%. The yield stress and Young's modulus of steel were 248.2 MPa and $2\times10^5$ MPa, respectively.

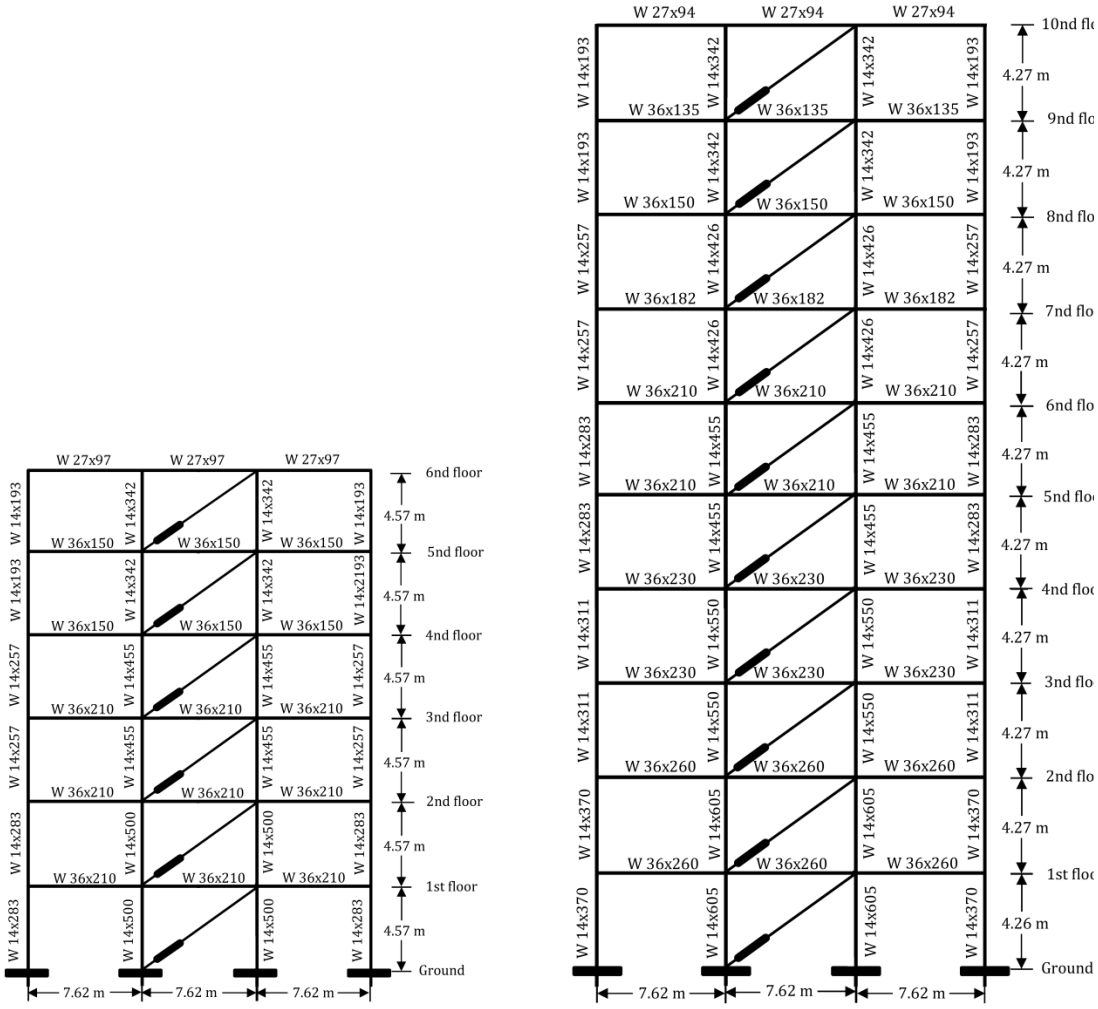


(a) 6-story [55] (b) 10-story [6]

Figure 2: The model of SMRFs equipped with FDDBs adopted in this study

Modeling the inelastic SMRFs and the nonlinear time-history analysis were conducted in the open-source finite element software OpenSEES [56]. The lumped plasticity approach was adopted for the nonlinear behavior of beams and columns. For this end, the plastic hinge

at the ends of elastic beams and columns was modeled by a zero-length element. The modified Ibarra-Medina-Krawinkler (IMK) deterioration model with pinching hysteretic response [57] was assigned to the plastic hinges. The Rayleigh damping model was used to define the damping matrix of the SMRF equipped with FDDBs. Two numerical evaluations of the structural responses were adopted to validate modeling the SMRFs in this study. First, the natural period of vibration corresponding to the fundamental mode of the structures was computed and reported in Table 1.

Table 1: Comparison of the natural period of fundamental mode

| SMRF | Natural period (s) | | Difference (%) |
|---|---|---|---|
| | Reference | Present study | |
| 6-story | 1.22 [55] | 1.18 | 3.28 |
| 10-story | 1.50 [6] | 1.49 | -0.67 |

The results given in Table 1 indicated that the natural period of fundamental mode was close to that reported by Wong [55] and Wong and Johnson [6]. In addition, the cumulative hysteresis energy of the 6- and 10-story SMRFs was respectively calculated under the record of the 1994 Northridge and 1995 Kobe earthquakes and compared with that of references [55, 6]. The cumulative hysteresis energy of the SMRFs was shown in Table 2. Therefore, these results shown in Table 2 verified modeling the SMRFs and the numerical method (expressed in section 3.2) used in this study.

Table 2: Comparison of the cumulative hysteresis energy of SMRFs

| SMRF | Cumulative hysteresis energy (kJ) | | Difference (%) |
|---|---|---|---|
| | Reference | Present study | |
| 6-story | 2,580 [55] | 2,540 | -1.55 |
| 10-story | 3,665 [6] | 3,681 | 0.40 |

To model the BFDS in OpenSEES [56], the process of modeling the BFDS proposed by Morales Ramirez [11] was adopted and used in this study. It is noted that in this study, the stick-slip and the slipping (or sliding) phases were considered for modeling the BFDS, and the slip-lock phase was ignored. In this method, the brace behavior in tension and compression cases was simulated using the truss element with the uniaxial Steel02 material. In addition, a zero-length element was considered for modeling the friction damper. The uniaxial BoucWen material was chosen to simulate the hysteresis behavior of friction damper in the stick-slip and slipping phases. Since all past studies for the optimization design and assessment of the friction dampers haven't considered the slip-lock phase, the phase wasn't model in the optimization process of this study.

## 7. RESULTS AND DISCUSSION

Details of the selection and scaling of earthquake records, the optimal design of the BFDSs, and the fragility assessment results of the optimized BFDSs-controled 6- and 10-story SMRFs are presented in this section.

### *7.1. Selection and scaling of earthquake records*

The design of a passive system is strongly dependent on earthquake excitations. Hence, the selection of earthquake records has been considered as a substantial challenge in the design of a passive system [58]. The seismic provisions of building codes such as ASCE/SEI 7-16 offer the selection of at least seven pairs of ground motion excitations for representing the seismic hazard of the site. Due to the high computational cost of the optimal design of the BFDSs for the seismic control of a large inelastic building, the 6- and 10-story SMRFs were first analyzed under the 22 far-field ground motion records given in FEMA-P695 [50]. Then, the seven records (Table 3) were selected for the optimum design of the BFDSs, which caused the high values of $DI_{\text{overall}}$. The main characteristics of the strong ground-motion records used in this study were listed in Table 3. For each earthquake, the main horizontal component with larger PGA was selected as the strong component.

Table 3: Far-field ground motion records selected in the optimization procedure [50]

| No | Name | Year | Station | Magnitude | PGA (g) | PGV (cm/s) |
|---|---|---|---|---|---|---|
| 1 | Landers, USA (1) | 1992 | Yermo Fire Station | 7.3 | 0.24 | 52 |
| 2 | Landers, USA (2) | 1992 | Coolwater | 7.3 | 0.42 | 42 |
| 3 | Duzce, Turkey | 1999 | Bolu | 7.1 | 0.82 | 62 |
| 4 | Cape Mendocino, USA | 1992 | Rio Dell Overpass | 7.0 | 0.45 | 44 |
| 5 | Northridge, USA | 1994 | Canyon Country | 6.7 | 0.48 | 63 |
| 6 | Imperial Valley, USA | 1979 | El Centro Array #11 | 6.5 | 0.38 | 33 |
| 7 | Superstition Hills, USA | 1987 | Poe Road (temp) | 6.5 | 0.45 | 36 |

In this study, the optimal design of the BFDSs was conducted under the scaled earthquake records (Table 3). Due to no existing the information of the soil conditions of the sites correspond to the 6- and 10-story SMRFs, the earthquake records were not scaled to match a design response spectrum. In this study, scaling the earthquake records was implemented so that the value of their 5%-damped spectral acceleration at the fundamental period, $S_a(T_1, 5\%)$, of the structures was equal to 1.0 g [58].

### *7.2. Optimal design of the BFDSs*

For the optimum design of the BFDSs, $SR_{\min}, SR_{\max}, \overline{F}_{\min}$, and $\overline{F}_{\max}$ were respectively set at 1.0, 5.0, 0.1 (10%), and 1.0 (100%), which were recommended by Taiyari et al. [27]. The $DI_{\text{all}}$ value is commonly left to the discretion of the design engineer. Here, it was assumed to be 0.30. The particle swarm optimization algorithm with passive congregation, called PSOPC, [46] was used in this study. The population size of the PSOPC algorithm was to 30, and the maximum number of iterations of the PSOPC algorithm was selected to 200. The bounds of the inertia weight were assumed to 0.1 and 0.4. These values were selected based on the authors' experience and recommendations of the literature [59, 60, 42]. The optimum parameters of the BFDSs for the 6- and 10-story SMRFs obtained by the PSOPC algorithm

were presented in Table 4. Due to the algorithm' stochastic nature, ten independent runs were carried out, and then the values correspond to the minimum objective function among the ten runs were considered as the optimum design of the BFDSs.

Table 4: The optimum value of the BFDSs parameters

| Story level | 6-story SMRF | | 10-story SMRF | |
|---|---|---|---|---|
| | *SR* | $\bar{F}$ (%) | *SR* | $\bar{F}$ (%) |
| 1 | 3.136 | 60.27 | 2.988 | 65.76 |
| 2 | 4.440 | 80.84 | 4.225 | 75.51 |
| 3 | 3.098 | 31.21 | 2.262 | 40.04 |
| 4 | 2.922 | 62.78 | 3.291 | 67.0 |
| 5 | 2.457 | 15.16 | 2.221 | 46.72 |
| 6 | 4.655 | 52.87 | 3.338 | 69.16 |
| 7 | - | - | 3.808 | 34.81 |
| 8 | - | - | 4.250 | 56.51 |
| 9 | - | - | 3.029 | 56.37 |
| 10 | - | - | 3.886 | 30.60 |

Figure 3 shows the comparison of the distribution of the $DI_{story}$ mean values under the seven scaled earthquake records along the height of the uncontrolled (w/o BFDS) and controlled (w/ BFDS) SMRFs. Results show that the optimized BFDSs considerably reduced the damage index of stories, especially the 1th, 4th, and 5th stories of the 6-story SMRF, and the 1th to 8th stories of the 10-story SMRF. In fact, considering the difference of the $DI_{story}$ mean values as the constraint of the optimization problem efficiently provided the uniform distribution of the seismic damage in the controlled structures.

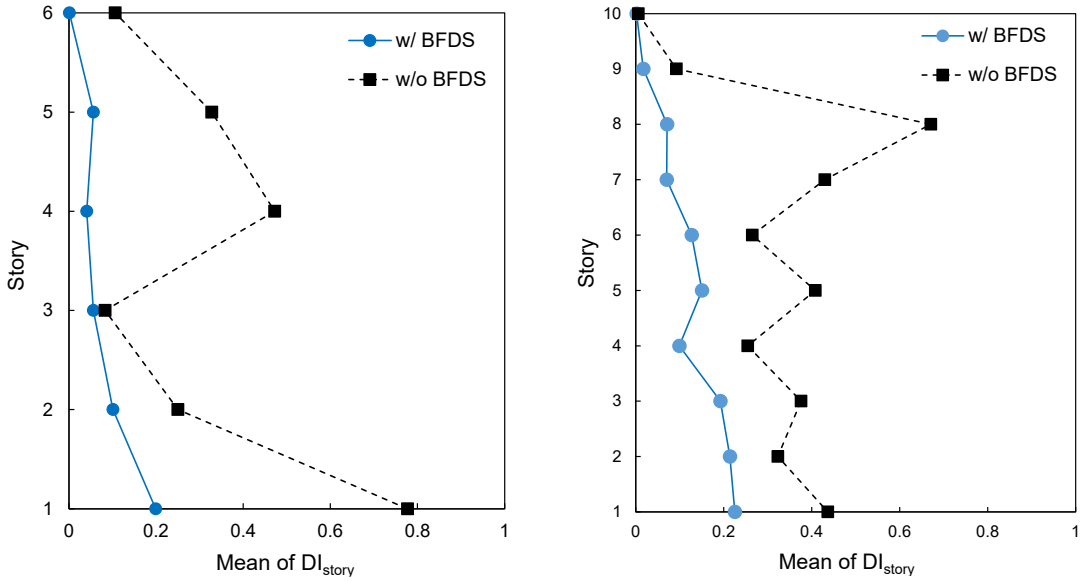


(a) 6-story (b) 10-story

Figure 3: Comparison of $DI_{story}$ mean value over the height of the uncontrolled and controlled SMRFs under the seven scaled earthquake records

The mean values of $DI_{\text{story}}$ shown in Figure 3 were reported in Table 5. As can be observed from Table 5, the maximum value of mean $DI_{\text{story}}$ for the 6- and 10-story SMRFs controlled by the optimized BFDSs was, respectively, 74.47% and 58.42% less than that of the uncontrolled SMRFs. Also, the variance of the mean $DI_{\text{story}}$ for the 6- and 10-story SMRFs controlled by the optimized BFDSs was, respectively, 95.06% and 82.38% less than that of the uncontrolled SMRFs. The reduction of the variance of mean $DI_{\text{story}}$ over the height indicate that the optimized BFDSs efficiently provide the uniform distribution of damage over the height of the structures.

Table 5: Comparison of mean values of $DI_{story}$ in the uncontrolled and controlled SMRFs averaged over seven scaled earthquake records

| Story level | 6-story SMRF | | 10-story SMRF | |
|---|---|---|---|---|
| | w/o BFDS | w/ BFDS | w/o BFDS | w/ BFDS |
| 1 | 0.777 | 0.199 | 0.436 | 0.225 |
| 2 | 0.25 | 0.1012 | 0.323 | 0.214 |
| 3 | 0.083 | 0.056 | 0.376 | 0.192 |
| 4 | 0.472 | 0.041 | 0.254 | 0.099 |
| 5 | 0.328 | 0.056 | 0.408 | 0.150 |
| 6 | 0.106 | 0.001 | 0.265 | 0.127 |
| 7 | - | - | 0.429 | 0.070 |
| 8 | - | - | 0.671 | 0.070 |
| 9 | - | - | 0.092 | 0.017 |
| 10 | - | - | 0.006 | 0.002 |
| Maximum | 0.777 | 0.199 (74.40%)* | 0.671 | 0.225 (58.42%) |
| Mean | 0.336 | 0.076 (77.47%) | 0.326 | 0.117 (64.15%) |
| Variance | 0.056 | 0.004 (93.06%) | 0.032 | 0.006 (82.38%) |

* Percentage reduction w/ FDDB (controlled) to w/o FDDB (uncontrolled)

The mean value of $DI_{\text{overall}}$ for the uncontrolled and controlled SMRFs under the seven earthquake records was shown in Table 6. Results indicate that the mean value of $DI_{\text{overall}}$ of the 6- and 10-story SMRFs equipped by the optimized BFDSs was respectively down 71.62% and 52.26% from that of the uncontrolled SMRFs.

Table 6: Comparison of mean values of $DI_{overall}$ of the uncontrolled and controlled SMRFs averaged over scaled earthquake records

| SMRF | w/o BFDS | w/ BFDS | Reduction (%) |
|---|---|---|---|
| 6-story | 0.613 | 0.174 | 71.62 |
| 10-story | 0.442 | 0.211 | 52.26 |

Figure 4 Figure 5 shows the comparison of the maximum value of the mean drifts and accelerations under the seven scaled earthquake records along the height of the uncontrolled and controlled SMRFs, respectively. Figure 4 indicates that the optimized BFDSs mitigate the maximum value of the mean drift of stories. As can be seen in from Figure 5, the optimized BFDSs provide the reduction of the maximum value of the mean acceleration in the stories of the 6-story SMRF, while the increase of these responses is shown in the stories

of the 10-story SMRF equipped with the optimized BFDSs. It is noted that in the controlled 10-story SMRF the maximum increase of the mean acceleration is occurred by about 15% (in 9$^{th}$ story). The more favorable effect of the friction damper system in decreasing the drift response than the reduction of the acceleration response was reported in literature [33].

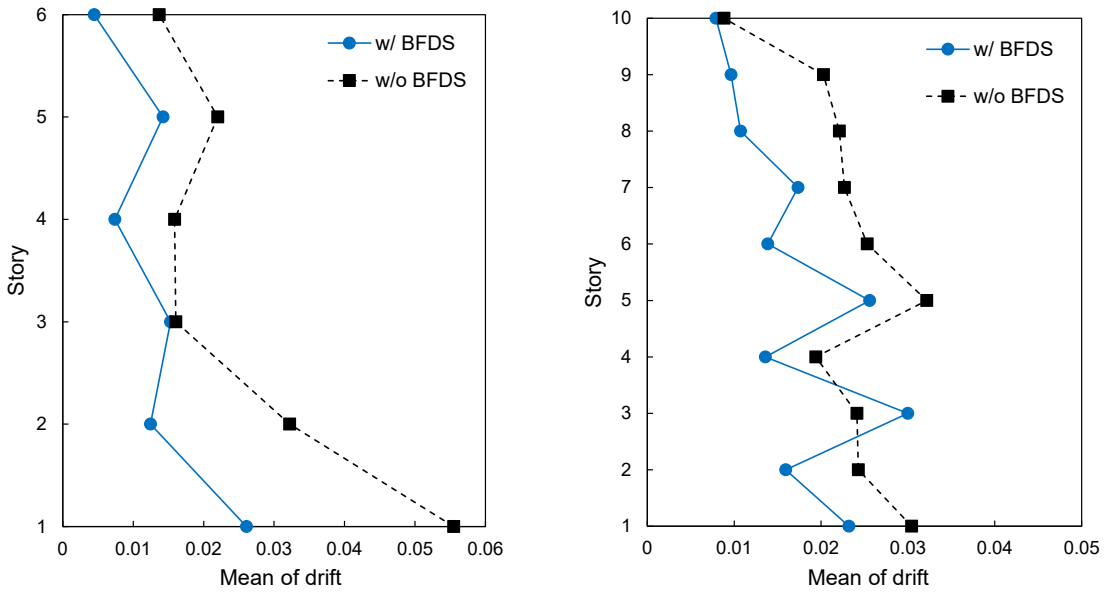


(a) 6-story (b) 10-story

Figure 4: Comparison of the maximum value of the mean drifts over the height of the uncontrolled and BFDSs-equipped SMRFs under the seven scaled earthquake records

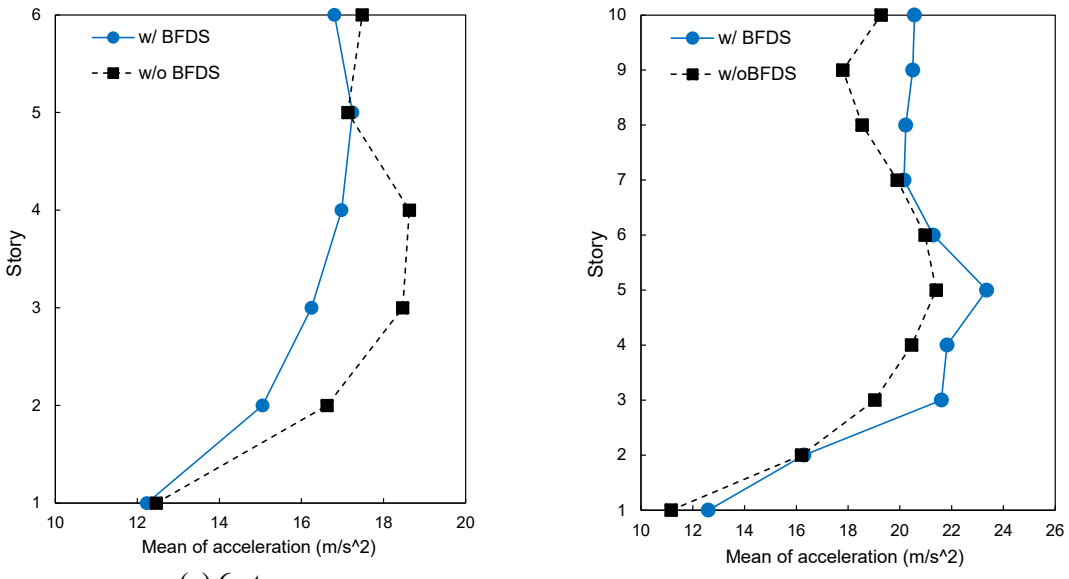


(a) 6-story (b) 10-story

Figure 5: Comparison of the maximum value of the mean accelerations over the height of the uncontrolled and BFDSs-equipped SMRFs under the seven scaled earthquake records

*7.3. Seismic fragility assessment*

The curves of the incremental dynamic analysis (IDA) of the 6- and 10-story SMRFs in the controlled and uncontrolled conditions were first obtained under the 22 far-field earthquake records given in FEMA-P695 [50]. Then, the 16%, 50%, and 84% fractile IDA curves shown in Figure 6 were constructed. Comparison of the fractile IDA curves for the different damage states allows for assessing the structure's adequacy to resist both frequent, small ground motions and rare, highly destructive earthquake records. In Figure 6, at a given fractile, the curves associated with the uncontrolled SMRFs fell to the lowest, followed by those of the controlled SMRFs, indicating that increasingly higher PGAs are required to cause a given $DI_{\text{overall}}$ in the SMRFs as its form changes from uncontrolled to BFDSs-controlled. It is noted the value of $DI_{\text{overall}}$ is null (i.e., zero) in the elastic response range. Hence, the values of the fractile IDA curves (see Figure 6) corresponding to lower values of PGA are null.

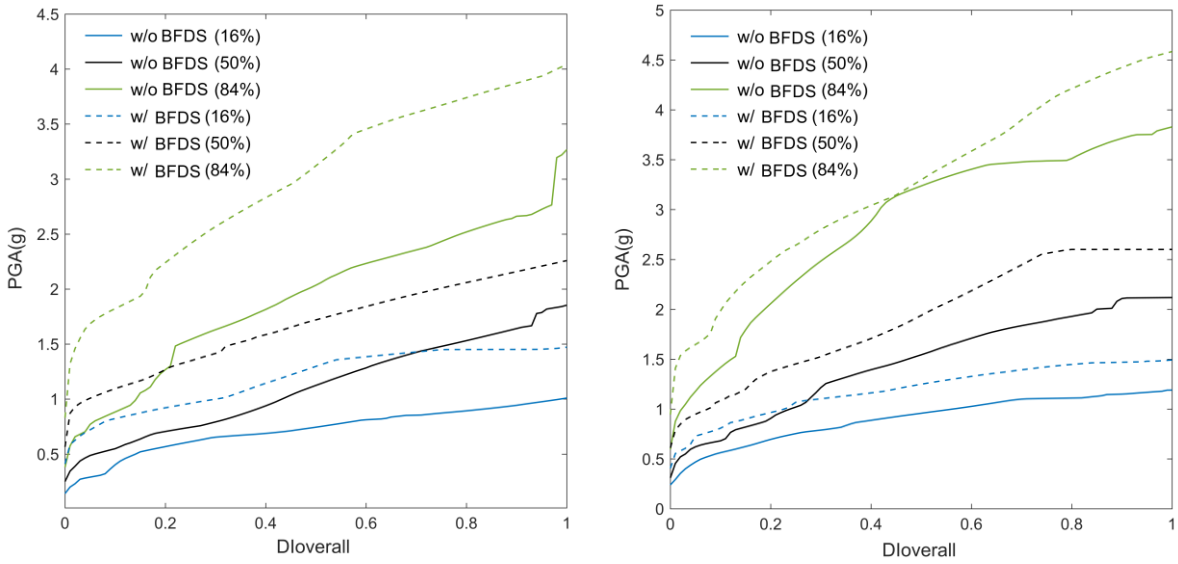


(a) 6-story (b) 10-story

Figure 6: 16, 50 and 84% fractals of IDA curves for the controlled and uncontrolled SMRFs

A similar observation is made from the fragility curves of the 6- and 10-story SMRFs shown in Figure 7Figure 8, respectively. At each of given damage states, the highest probability of failure is considered for the uncontrolled SMRF. For a better comparison of the seismic performance of the controlled and uncontrolled SMRFs, the results obtained from the fragility curves shown in Figure 7Figure 8 were reported in Table 7 for the PGA value corresponding to the mean $P_f$ (i.e., $P_f = 0.5$) for each of defined damage states. Results indicates that the uncontrolled SMRFs are associated with considerably greater PGA demands than controlled SMRFs in all the damage states. Therefore, the results of the seismic assessment demonstrate that the seismic retrofit of the SMRFs using the optimized BFDS devices can enhance the seismic performance of the SMRFs.

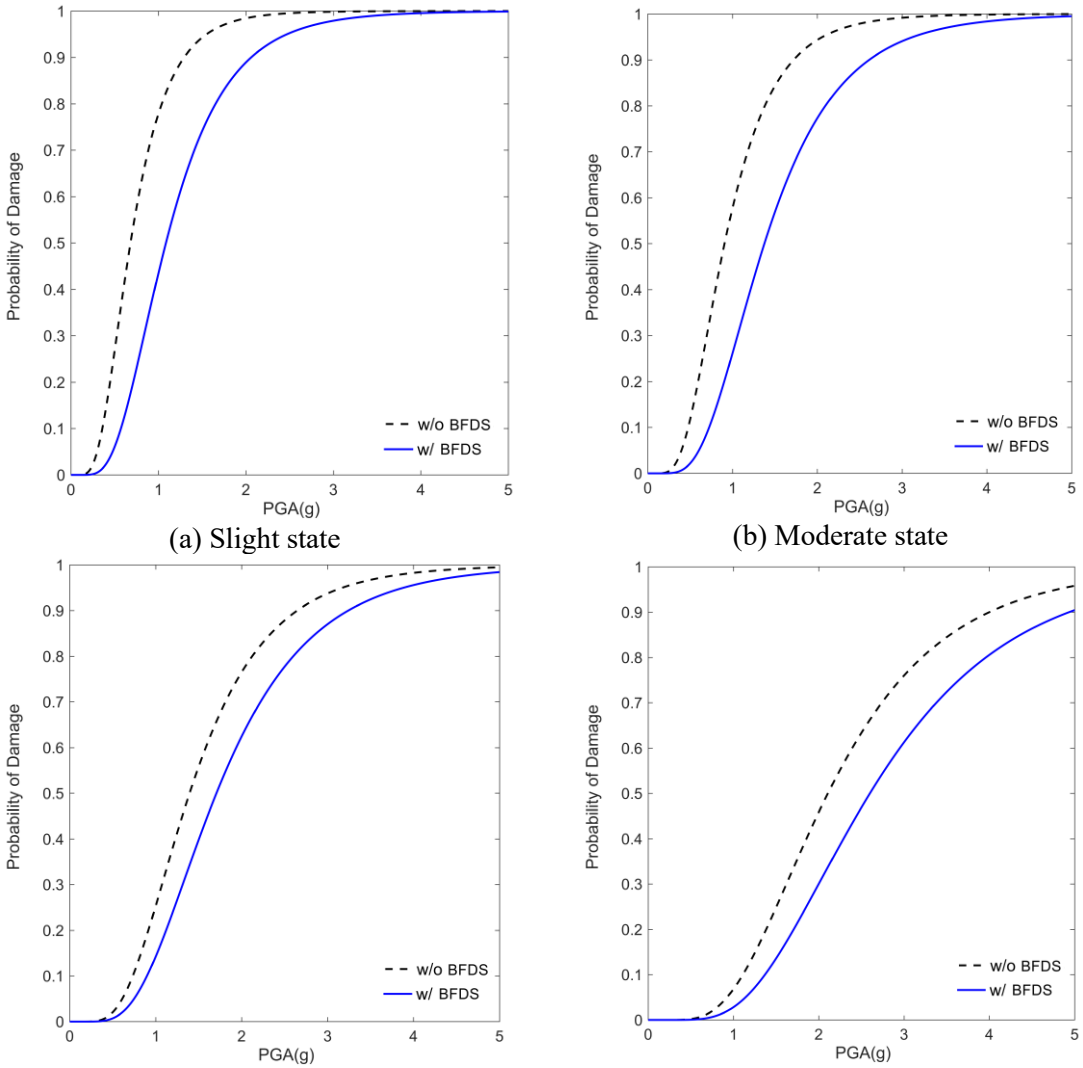


(a) Slight state (b) Moderate state

(c) Severe state (d) Complete state

Figure 7: Fragility curves for the controlled and uncontrolled 6-story SMRF in different damage states

## 8. CONCLUSIONS

This study focused on the optimum design of the bracing-friction damper systems (BFDSs) for the optimal seismic retrofit of the 6- and 10-story inelastic steel moment-resisting frames (SMRFs). For this end, the parameters of the BFDSs containing the stiffness ratio and the normalized slip force were optimized through minimizing the maximum damage index of stories of the BFDSs-equipped SMRF averaged over the seven scaled earthquake records. The optimization problem was constrained to look for solutions (systems) that exhibit uniformly distributed damage along the SMRF building height during earthquake excitation.

The optimal design of the BFDSs was achieved using the passive congregation particle swarm algorithm (PSOPC).

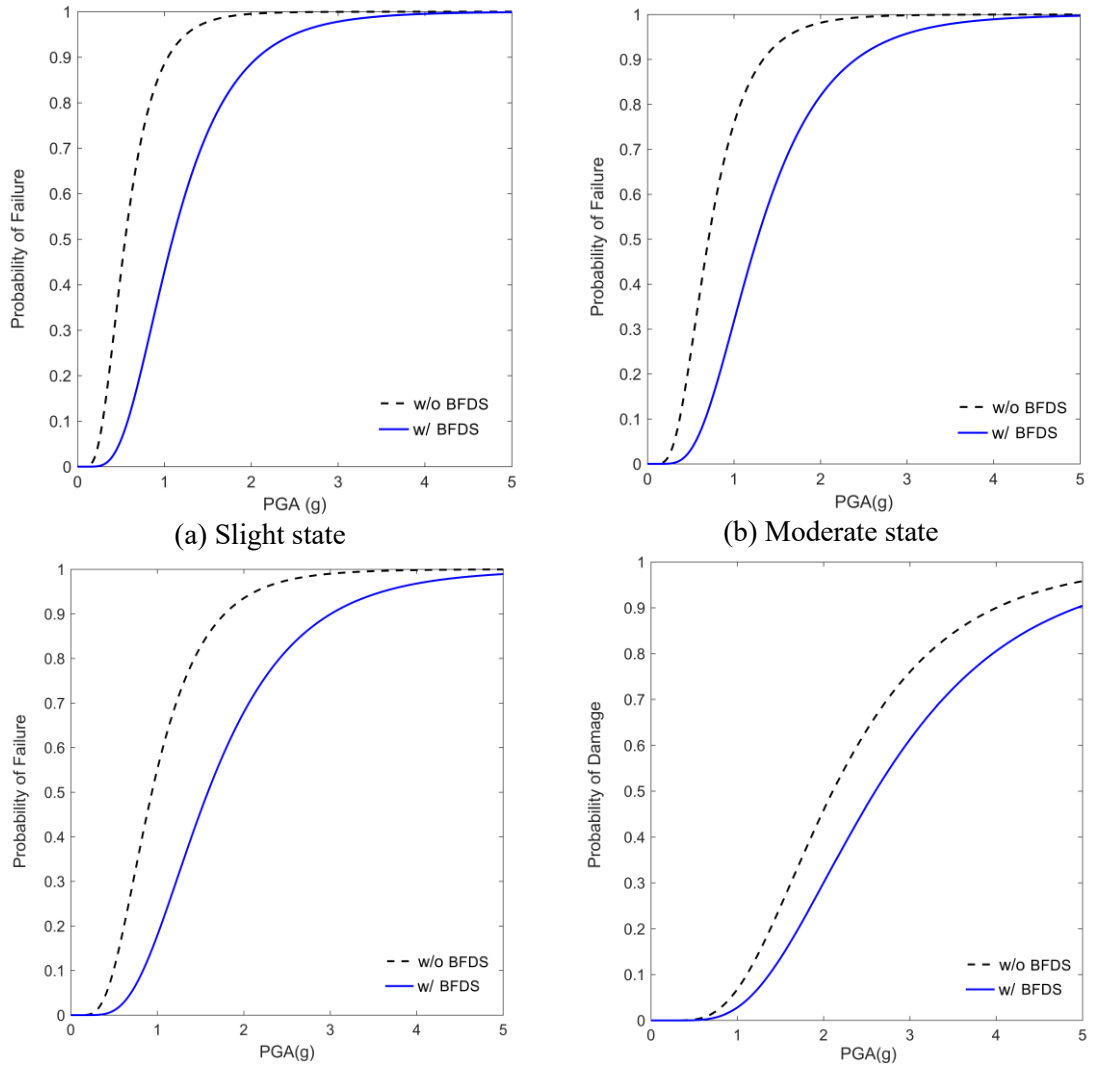


Figure 8: Fragility curves for the controlled and uncontrolled 10-story SMRF in different damage states

Table 7: Comparison of the PGA value corresponding to mean $P_f$ (i.e., $P_f = 0.5$)

| Damage state | 6-story | | | 10-story | | |
|---|---|---|---|---|---|---|
| | w/o BFDS | w/ BFDS | Change (%) | w/o BFDS | w/ BFDS | Change (%) |
| Slight | 0.55 | 1.1 | 100 | 0.69 | 1.09 | 57.9 |
| Moderate | 0.71 | 1.27 | 78.9 | 0.91 | 1.38 | 51.6 |
| Severe | 0.94 | 1.59 | 69.1 | 1.40 | 1.71 | 22.1 |
| Complete | 1.65 | 2.16 | 30.9 | 2.11 | 2.61 | 23.7 |

The optimization results indicated that the maximum value of the story damage index ($DI_{\text{story}}$) averaged over the seven scaled earthquake records for the 6- and 10-story SMRFs controlled by the optimized BFDSs was respectively reduced to 74.47% and 58.42% down from the uncontrolled SMRFs. The variance of the mean values of the maximum $DI_{\text{story}}$ for the 6- and 10-story SMRFs controlled by the optimized BFDSs was 95.06% and 82.38% less than that of the uncontrolled SMRFs, respectively. Thus, for the controlled SMRFs the distribution of damage was uniformly occurred over the height of the structures. In addition, the reduction of the overall damage, $DI_{\text{overall}}$, and drifts were concluded that the optimum design of the BFDSs could protect the inelastic SMRFs from suffering damages subjected to scaled seven earthquake excitations.

In the final phase of this study, the fragility concept was used to assess the seismic performance of the considered SMRFs with and without the optimized BFDSs at various damage states. The seismic fragility assessment of the structures was conducted based on IDA. The results of the seismic fragility assessment revealed that the seismic performance of the optimized BFDSs-equipped SMRFs is superior to that of the uncontrolled SMRFs at all considered damage states, reducing significantly structural and non-structural damage.

## REFERENCES

1. Kaveh A, Mohammadi S, Khademhosseini O, Keyhani A, Kalatjari V. Optimum parameters of tuned mass dampers for seismic applications using charged system search, *Iran. J. Sci. Technol. - Trans. Civ. Eng*. 2015; **39**:21–40. doi: 10.22099/ijstc.2015.2739.
2. Hojat Jalali H, Fahimi farzam M, Kaveh A. Statistical seismic performance assessment of tuned mass damper inerter, *Struct Control Health Monit*. 2020; **27**. doi:10.1002/stc.2602.
3. Kaveh A, Javadi SM, Mahdipour Moghanni R. Optimal structural control of tall buildings using tuned mass dampers via chaotic optimization algorithm, *Structures*. 2020; **28**:2704–13. doi:https://doi.org/10.1016/j.istruc.2020.11.002.
4. Khatibinia M, Ahrari A, Gharehbaghi S, Sarafrazi SR. An efficient approach for optimum shape design of steel shear panel dampers under cyclic loading, *Smart. Struct. Syst*. 2021; **27**(3):547–57. doi:https://doi.org/10.12989/sss.2021.27.3.547.
5. Gholizadeh S, Hasançebi O, Eser H, Koçkaya O. Seismic collapse safety based optimization of steel Moment-Resisting frames, *Structures*. 2022; **45**:329–42. doi:https://doi.org/10.1016/j.istruc.2022.09.034.
6. Wong KK, Johnson J. Seismic Energy Dissipation of inelastic structures with multiple tuned mass dampers, *J. Eng. Mech*. 2009; **135**(4):265–75. doi:10.1061/(ASCE)0733-9399(2009)135:4(265).
7. Jarrahi H, Asadi A, Khatibinia M, Etedali S. Optimal design of rotational friction dampers for improving seismic performance of inelastic structures, *J. Buil. Eng*. 2020; **27**:100960. doi:https://doi.org/10.1016/j.jobe.2019.100960.

8. Pall AS, Marsh C. Response of Friction Damped Braced Frames, *J. Struct. Div*. 1982; **108**(6):1313–23. doi:doi:10.1061/JSDEAG.0005968.
9. Grigorian CE, Yang TS, Popov EP. Slotted Bolted Connection Energy Dissipators. Earthquake Spectra. 1993;9(3):491–504. doi:10.1193/1.1585726.
10. Nims DK, Richter PJ, Bachman RE. The Use of the Energy Dissipating Restraint for Seismic Hazard Mitigation, *Earthq. Spectra*. 1993; **9**(3):467–89. doi:10.1193/1.1585725.
11. Morales JD. *Numerical simulations of steel frames equipped with friction-damped diagonal-bracing devices*, Concordia University; 2011.
12. Ramirez JM, Tirca L. Numerical simulation and design of friction-damped damped steel frame structures, *In Proceedings of the 15th World Conference on Earthquake Engineering*, 2012, Lisbon, Portugal, 24–28.
13. Wu B, Zhang J, Williams MS, Ou J. Hysteretic behavior of improved Pall-typed frictional dampers. *Eng. Struct*. 2005; **27**(8):1258–67. doi:https://doi.org/10.1016/j.engstruct.2005.03.010.
14. Aiken ID. *Earthquake simulator testing and analytical studies of two energy-absorbing systems for multistory structures*, Report UCB/EERC-90/03, University of California, Berkeley, 1990.
15. Mualla IH, Belev B. Performance of steel frames with a new friction damper device under earthquake excitation. *Eng. Struct*. 2002; **24**(3):365–71. doi:https://doi.org/10.1016/S0141-0296(01)00102-X.
16. Nabid N, Hajirasouliha I, Petkovski M. A practical method for optimum seismic design of friction wall dampers, *Earthq. Spectra*. 2017; **33**(3):1033–52. doi:10.1193/110316eqs190m.
17. FitzGerald TF, Anagnos T, Goodson M, Zsutty T. Slotted bolted connections in a seismic design for concentrically braced connections, *Earthq. Spectra*. 1989; **5**(2):383–91. doi:10.1193/1.1585528.
18. Monir HS, Zeynali K. A modified friction damper for diagonal bracing of structures, *J. Constr. Steel. Res*. 2013; **87**:17–30. doi:https://doi.org/10.1016/j.jcsr.2013.04.004.
19. Ebrahimi S, Mirghaderi SR. A new friction–slip brace damper to improve seismic performance of braced frames. *J. Constr. Steel. Res*. 2023; **207**:107945. doi:https://doi.org/10.1016/j.jcsr.2023.107945.
20. Latour M, Piluso V, Rizzano G. Free from damage beam-to-column joints: Testing and design of DST connections with friction pads, *Eng. Struct*. 2015; **85**:219–33. doi:https://doi.org/10.1016/j.engstruct.2014.12.019.
21. Latour M, D'Aniello M, Zimbru M, Rizzano G, Piluso V, Landolfo R. Removable friction dampers for low-damage steel beam-to-column joints. Soil Dynamics and Earthquake Engineering. 2018;115:66–81. doi:https://doi.org/10.1016/j.soildyn.2018.08.002.

22. Nastri E, D'Aniello M, Zimbru M, Streppone S, Landolfo R, Montuori R et al. Seismic response of steel moment resisting frames equipped with friction beam-to-column joints, *Soil. Dyn. Earthq. Eng.* 2019; **119**: 144-57. doi:https://doi.org/10.1016/j.soildyn.2019.01.009.
23. Shahini M, Sabbagh AB, Davidson P, Mirghaderi R. Development of cold-formed steel moment-resisting connections with bolting friction-slip mechanism for seismic applications, *Thin-Walled. Struct*. 2019; **141**:217–31. doi:https://doi.org/10.1016/j.tws.2019.04.011.
24. Seifan F, Mirghaderi SR, Ghassemieh M. A new friction-slip connection for moment frames with continuous beams, *J. Constr. Steel. Res*. 2020; **175**:106337. doi:https://doi.org/10.1016/j.jcsr.2020.106337.
25. Moreschi LM, Singh MP. Design of yielding metallic and friction dampers for optimal seismic performance, *Earthq. Eng. Struct. Dyn*. 2003; **32**(8):1291–311. doi:https://doi.org/10.1002/eqe.275.
26. Lee S-H, Park J-H, Lee S-K, Min K-W. Allocation and slip load of friction dampers for a seismically excited building structure based on storey shear force distribution, *Eng. Struct*. 2008; **30**(4):930–40. doi:https://doi.org/10.1016/j.engstruct.2007.03.020.
27. Taiyari F, Mazzolani FM, Bagheri S. Damage-based optimal design of friction dampers in multistory chevron braced steel frames, *Soil. Dyn. Earthq. Eng.* 2019; **119**:11–20. doi:https://doi.org/10.1016/j.soildyn.2019.01.004.
28. Ghorbani HR, Rofooei FR. A novel double slip loads friction damper to control the seismic response of structures, *Eng. Struct*. 2020; **225**:111273. doi:https://doi.org/10.1016/j.engstruct.2020.111273.
29. Jarrahi H, Asadi A, Khatibinia M, Etedali S, Samadi A. Simultaneous optimization of placement and parameters of rotational friction dampers for seismic-excited steel moment-resisting frames, *Soil. Dyn. Earthq. Eng.* 2020; **136**:106193. doi:https://doi.org/10.1016/j.soildyn.2020.106193.
30. Moghaddam H, Afzalinia F, Hajirasouliha I. Optimal distribution of friction dampers to improve the seismic performance of steel moment resisting frames, *Structures*. 2022; **37**:624–44. doi:https://doi.org/10.1016/j.istruc.2022.01.007.
31. Lukkunaprasit P, Wanitkorkul A, Filiatrault A, Performance deterioration of slotted-bolted connection due to bolt impact and remedy by restrainers. *In Thirteenth World Conference on Earthquake Engineering,* 2004.
32. Baktash P, Marsh C, editors. Seismic behavior of friction damped braced frames, *Proceedings of the third US National Conference on Earthquake Engineering*, Charleston, SC; 1986.
33. Lee S-K, Park J-H, Moon B-W, Min K-W, Lee S-H, Kim J. Design of a bracing-friction damper system for seismic retrofitting. *Smart. Struct. Syst*. 2008; **4**: 685-96. doi:10.12989/sss.2008.4.5.685.

34. Ghobarah A, Abou-Elfath H, Biddah A. Response-based damage assessment of structures, E *Earthq. Eng. Struct. Dyn*. 1999; **28**(1):79–104. doi:https://doi.org/10.1002/(SICI)1096-9845(199901)28:1<79::AID-EQE805>3.0.CO;2-J.
35. Bozorgnia Y, Bertero VV. Evaluation of damage Potential of recorded earthquake ground motion, *Seismol. Res. Lett*. 2001; **72**.
36. Williams MS, Sexsmith RG. Seismic damage indices for concrete structures: a state-of-the art review, *Earthq. Spectra*. 1995; **11**(2):319–49. doi:10.1193/1.1585817.
37. Kunnath SK, Reinhorn AM, Lobo RF, editors. IDARC Version 3.0: A Program for the Inelastic Damage Analysis of Reinforced Concrete Structures1992.
38. Reinhorn A, Roh H, Sivaselvan M, Kunnath S, et al. IDARC 2D Version 7.0: A Program for the Inelastic Damage Analysis of Structures. 2009.
39. Park YJ, Ang AHS. Mechanistic Seismic Damage Model for Reinforced Concrete, *J. Struct. Eng*. 1985; **111**(4):722–39. doi:10.1061/(ASCE)0733-9445(1985)111:4(722).
40. Ghosh S, Datta D, Katakdhond AA. Estimation of the Park–Ang damage index for planar multi-storey frames using equivalent single-degree systems, *Eng. Struct*. 2011; **33**(9):2509–24. doi:https://doi.org/10.1016/j.engstruct.2011.04.023.
41. Gong Y, Xue Y, Xu L. Optimal capacity design of eccentrically braced steel frameworks using nonlinear response history analysis, *Eng. Struct*. 2013; **48**:28–36. doi:10.1016/j.engstruct.2012.10.001.
42. Gharehbaghi S. Damage controlled optimum seismic design of reinforced concrete framed structures. *Struct. Eng. Mech*. 2018; **65**:53–68. doi:10.12989/sem.2018.65.1.053.
43. Coello Coello CA. Theoretical and numerical constraint-handling techniques used with evolutionary algorithms: a survey of the state of the art, *Comput. Methods Appl. Mech. Eng*. 2002; **191**(11):1245–87. doi:https://doi.org/10.1016/S0045-7825(01)00323-1.
44. Kaveh A, Zolghadr A. Truss optimization with natural frequency constraints using a hybridized CSS-BBBC algorithm with trap recognition capability, *Comput*. *Strut*. 2012; **102-103**:14–27. doi:https://doi.org/10.1016/j.compstruc.2012.03.016.
45. Kaveh A. Advances in metaheuristic algorithms for optimal design of structures. Springer Cham, 3rd ed., 2021.
46. He S, Wu QH, Wen JY, Saunders JR, Paton RC. A particle swarm optimizer with passive congregation, *Biosystems*. 2004; **78**(1):135–47. doi:https://doi.org/10.1016/j.biosystems.2004.08.003.
47. Vamvatsikos D, Cornell CA. Incremental dynamic analysis, *Earthq. Eng. Struct. Dyn*. 2002; **31**(3):491–514. doi:https://doi.org/10.1002/eqe.141.
48. Lignos DG, Kolios D, Miranda E. Fragility Assessment of Reduced Beam Section Moment Connections, *J. Struct. Eng*. 2010; **136**(9):1140–50. doi:doi:10.1061/(ASCE)ST.1943-541X.0000214.

49. Jalayer F, Cornell CA. A technical framework for probability-based demand and capacity factor design (DCFD) seismic formats, Pacific Earthquake Engineering Research Center; 2004.
50. Council AT, Agency USFEM. *Quantification of building seismic performance factors. US Department of Homeland Security*, FEMA; 2009.
51. Tirca L, Chen L, Tremblay R. Assessing collapse safety of CBF buildings subjected to crustal and subduction earthquakes, *J. Constr. Steel. Res*. 2015; **115**:47–61. doi:https://doi.org/10.1016/j.jcsr.2015.07.025.
52. Cosenza E, Manfredi G. Damage indices and damage measures. *Progress in Structural Engineering and Materials*. 2000; **2**(1):50–9. doi:https://doi.org/10.1002/(SICI)1528-2716(200001/03)2:1<50::AID-PSE7>3.0.CO;2-S.
53. Park Y-J, Ang AH-S, Wen YK. Seismic damage analysis of reinforced concrete buildings. *J. Struct. Eng*. 1985; **111**(4):740–57.
54. Pujades LG, Vargas-Alzate YF, Barbat AH, González-Drigo JR. Parametric model for capacity curves, *Bull. Earth. Eng*. 2015; **13**(5):1347–76. doi:10.1007/s10518-014-9670-5.
55. Wong KK. Seismic Energy Dissipation of Inelastic Structures with Tuned Mass Dampers. *J. Eng. Mech*. 2008; **134**(2):163–72. doi:doi:10.1061/(ASCE)0733-9399(2008)134:2(163).
56. McKenna F. OpenSees: A Framework for Earthquake Engineering Simulation. Computing in Science & Engineering. 2011;13:58–66. doi:10.1109/MCSE.2011.66.
57. Ibarra LF, Medina RA, Krawinkler H. Hysteretic models that incorporate strength and stiffness deterioration, *Earthq. Eng. Struct. Dyn*. 2005; **34**(12):1489–511. doi:https://doi.org/10.1002/eqe.495.
58. Khatibinia M, Akbari S, Yazdani H, Gharehbaghi S. Damage-based optimal control of steel moment-resisting frames equipped with tuned mass dampers. *J. Vib. Control*. 30: **3**-**4**: 659-672. doi:10.1177/10775463221149462.
59. Shayesteh Bilondi MR, Yazdani H, Khatibinia M. Seismic energy dissipation-based optimum design of tuned mass dampers, *Struct. Multidiscip. Optim*. 2018; **58**(6):2517–31. doi:10.1007/s00158-018-2033-0.
60. Khatibinia M, Jalaipour M, Gharehbaghi S. Shape optimization of U-shaped steel dampers subjected to cyclic loading using an efficient hybrid approach, *Eng. Struct*. 2019;197:108874. doi:https://doi.org/10.1016/j.engstruct.2019.02.005.